Localizing Sources Using a Network of Asynchronous Compact Arrays

Ildar R. Urazghildiiev and David E. Hannay

***Abstract*—This paper considers the problem of passive acoustic localization of sources using a network of stationary compact arrays of acoustic sensors providing azimuth and elevation measurements of detected sounds. The maximum-likelihood estimator and Cramér–Rao bounds are derived. The localization accuracy is evaluated using statistical simulations and *in situ* tests. The plots of azimuth, range, and position estimation accuracy are presented. Test results demonstrated that superefficient position estimates with an error lower than the Cramér–Rao bounds can be achieved for surface vessels and other sound sources with known depths.**

***Index Terms*—Compact array, estimation errors, maximum-likelihood (ML) estimator, source localization.**

I. Introduction

DESPITE the technical complexity of using stationary compact arrays of acoustic sensors, they are becoming more widespread in underwater passive acoustics because they can measure the azimuth and elevation angles of detected sounds [1]–[9]. Because of the small dimensions of compact arrays, they are unsuitable for practical range measurements [8]. However, compact arrays can be used for estimating ranges if they are configured in a spatially distributed network. If a source is detected by two or more compact arrays that are not located on the same line with the source, the source's azimuth, elevation, and range are observable from the azimuth and elevation measurements provided by the compact arrays. In practice, a network of two or more underwater compact arrays can ensure unambiguous localization of surface vessels, marine animals, and other sound producing sources within large marine areas. This capability can be used to monitor coastal and offshore vessel activities in marine protected areas and conservation areas, where other tracking methods, such as RADAR or automatic identification systems (AIS), are ineffective.

Applying two compact arrays to estimate ranges of vessels is considered in [2]. When the arrays were 100 m apart, the position estimation accuracy was about 7% within a vessel-to-array range of 250 m. However, the closed-form representations of the localization algorithms used in that system were not given in [2].

The problem of localizing and tracking sources from multiple bearing measurements provided by radar sensors is considered in [10] and [11]. The triangulation algorithms considered in these works could potentially be applied in underwater acoustics. However, the propagation of underwater sound is obviously different from the propagation of electromagnetic waves in air in terms of the present surface and bottom reflections, refraction, multipath propagation, and other unpredictable effects. Besides this, the speeds and trajectories of surface vessels and marine animals are different from those of the sources of interest for radar applications. Therefore, the potential and actual localization accuracy provided by a network of underwater compact arrays is of great theoretical and practical interest.

This paper considers the problem of estimating the positions of sources using azimuth and elevation measurements from a network of stationary compact arrays. The goals of this paper are to derive the maximum-likelihood (ML) position estimator, derive the closed-form representations for the Cramér–Rao bounds (CRBs), and evaluate the position estimation accuracy provided by the various array locations using statistical simulations and *in situ* tests. The *in situ* tests were conducted using two stationary compact tetrahedral arrays of recorders designed by JASCO Applied Sciences, which were deployed in the Strait of Georgia near Vancouver, BC, Canada. The main contributions of this work are the closed-form representations for the ML estimator and the CRBs, as well as test results representing the estimation accuracy in real-world scenarios. The intended applications of the technique considered in this work include, but are not limited to, passive acoustic detection, localization and tracking vessels and marine animals, and estimation of population densities and abundances. The results of this work can be used for preliminary evaluations of a system's effectiveness at the design stage and for testing the feasibility of specific requirements. Section II considers a data model and problem formulation. Section III presents the closed-form representations of the ML estimator. Section IV derives representations for the CRB. Section V presents the results of simulations and *in situ* tests.

II. Data Model and Problem Formulation

We assume that vessels, marine mammals, and other sources of interest are presented as point sources such that the source position is specified by the average position of the sound generating components [9]. Spatial coordinates of the sources are specified in a 3-D Cartesian coordinate

Manuscript received July 3, 2018; revised February 8, 2019; accepted May 2, 2019. *(Corresponding author: Ildar R. Urazghildiiev.)*

Associate Editor: Z.-H. Michalopoulou.

I. R. Urazghildiiev is with JASCO Applied Sciences (USA), Inc., Silver Spring, MD 20910 USA (e-mail: ildar.urazghildiiev@jasco.com).

D. E. Hannay is with JASCO Applied Sciences (Canada) Ltd., Victoria, BC V8Z 7X8, Canada (e-mail: david.hannay@jasco.com).

Digital Object Identifier 10.1109/JOE.2019.2915913

system with axes *X* and *Y* placed in a horizontal plane and axis *Z* oriented upward. The vector of source position is defined as follows:

$$\boldsymbol{r}_S = \begin{bmatrix} x_S \\ y_S \\ z_S \end{bmatrix} = r_S \begin{bmatrix} \sin\alpha_S \, \cos\beta_S \\ \cos\alpha_S \, \cos\beta_S \\ \sin\beta_S \end{bmatrix} \in R^3 \tag{1}$$

where $r_S = \|\boldsymbol{r}_S\|$ is a slant distance to the source, α_S is the source azimuth, and β_S is the source elevation angle. From (1), it follows that an unknown source position can be represented either in rectangular coordinates as vector $\boldsymbol{r}_S$ (1) or in polar coordinates as a vector

$$\boldsymbol{\gamma}_S = [\alpha_S, \beta_S, r_S]^T \in R^3. \tag{2}$$

Here and elsewhere the symbol "*T*" denotes transpose.

It is assumed that a network of $N \geq 2$ compact arrays is used to localize a source. Each compact array consists of a small number of synchronized hydrophones with the distance between them typically from 0.5 to 2 m [2], [4], [6], [8], [9], [12]–[14]. The size of arrays is much smaller than the distance between the closest arrays such that the position of the *n*th compact array is specified by the vector $\boldsymbol{r}_n = [x_n, y_n, z_n]^T \in R^3$, $n = 1 \ldots N$, as the position of its center.

Each compact array provides the measurements of azimuth α_n and elevation angle β_n of the source. The bearings α_n and β_n are defined in a rectangular coordinate system associated with the nth array. They are obtained by transferring the original coordinate system into the point $\boldsymbol{r}_n$ such that

$$\alpha_n = \tan^{-1}\frac{x_S - x_n}{y_S - y_n}, \quad \beta_n = \tan^{-1}\frac{z_S - z_n}{d_{Sn}}. \tag{3}$$

Here, $d_{Sn} = \sqrt{(x_S - x_n)^2 + (y_S - y_n)^2}$ is the horizontal distance to the source relative to the nth array.

The bearing estimates are

$$\hat{\alpha}_n = \alpha_n + \varepsilon_{\alpha n}, \quad \hat{\beta}_n = \beta_n + \varepsilon_{\beta n}, \quad n = 1 \ldots N \tag{4}$$

where $\varepsilon_{\alpha n}$ is the azimuth and $\varepsilon_{\beta n}$ is the elevation estimation error. An example of time-difference-of-arrival (TDOA)-based ML estimator of bearings (3) applicable to compact arrays is given in [8], but other array processing techniques, such as various kinds of beamformers considered in [15], can also be applied.

The statistical distribution of bearing estimation errors is unknown, but it depends on many independent factors, such as the sound propagation environment, the presence of bottom and surface reflections, technical characteristics and deployment of the array, the bearing estimation algorithm used to compute (4), signal-to-noise ratio (SNR), and others. Considering the influence of all these factors on the statistical properties of the bearing estimates was outside the scope of this work. However, under the presence of multiple independent factors, the Gaussian random variable can be used to model the measurement errors. Therefore, for the sake of simplicity, we make a standard assumption that the measurement errors $\varepsilon_{\alpha n}$ and $\varepsilon_{\beta n}$ are independent identically distributed (i.i.d.) Gaussian variables with zero mean and known variances σ_α^2 and σ_β^2. We assumed that SNR was high enough to detect sources at each compact array and to provide the variances $\sigma_\alpha^2, \sigma_\beta^2 < 1^\circ \ldots 3^\circ$ [8], [9]. In practice, the actual values of variances σ_α^2 and σ_β^2 provided by a single array can be evaluated from direct bearing measurements of sources with known coordinates [8], [9].

The compact arrays can be asynchronous in the sense that they measure bearings (3) of a source at different time instances $t_1 \neq t_2 \neq \cdots t_N$. However, it is assumed that the maximum time difference between N measurements (4) is negligibly small such that at any t_n, the source position can be represented by the vector $\boldsymbol{r}_S$. The problems considered in this paper are formulated as follows.

1) To obtain the closed-form representations for the ML estimators of the vectors $\boldsymbol{r}_S$ (1), $\boldsymbol{\gamma}_S$ (2), and for the corresponding CRBs approximating estimation errors.
2) To evaluate the accuracy of the ML estimates of the vectors $\boldsymbol{r}_S$ and $\boldsymbol{\gamma}_S$ using statistical simulations and *in situ* tests.

III. ML Estimator and CRBs

Considering (4), the available bearing measurements provided by a network of N compact arrays can be represented as a random vector given by

$$\hat{\boldsymbol{\theta}} = \boldsymbol{\theta} + \boldsymbol{\varepsilon} \ \in R^{2N} \tag{5}$$

where $\boldsymbol{\theta} = \boldsymbol{\theta}(\boldsymbol{r}_S) = \boldsymbol{\theta}(\boldsymbol{\gamma}_S) = [\boldsymbol{\alpha}^T, \boldsymbol{\beta}^T]^T \in R^{2N}$ is the vector of true bearings, $\boldsymbol{\alpha} = [\alpha_1, \ldots, \alpha_N]^T \in R^N$ and $\boldsymbol{\beta} = [\beta_1, \ldots, \beta_N]^T \in R^N$ are the vectors of source azimuths and elevation angles (3), and $\boldsymbol{\varepsilon} = [\varepsilon_{\alpha 1}, \ldots, \varepsilon_{\alpha N}, \varepsilon_{\beta 1}, \ldots, \varepsilon_{\beta N}]^T \in R^{2N}$ is the vector of measurement errors. The mean value and the covariance matrix of the observation vector (5) are as follows:

$$E\{\hat{\boldsymbol{\theta}}\} = \boldsymbol{\theta}$$

$$\boldsymbol{C} = E\left\{\left(\hat{\boldsymbol{\theta}} - \boldsymbol{\theta}\right)\left(\hat{\boldsymbol{\theta}} - \boldsymbol{\theta}\right)^T\right\} = \begin{bmatrix} \sigma_\alpha^2 \boldsymbol{I} & 0 \\ 0 & \sigma_\beta^2 \boldsymbol{I} \end{bmatrix} \in R^{2N \times 2N}. \tag{6}$$

Here, $\boldsymbol{I} \in R^{N \times N}$ is the unit matrix and $0 \in R^{N \times N}$ is the zero matrix.

The logarithmic-likelihood function of the vector $\hat{\boldsymbol{\theta}}$ is

$$\ln W(\hat{\boldsymbol{\theta}}|\boldsymbol{r}_S) = \ln W(\hat{\boldsymbol{\theta}}|\boldsymbol{\gamma}_S) = c - \frac{1}{2}(\hat{\boldsymbol{\theta}} - \boldsymbol{\theta})^T \boldsymbol{C}^{-1}(\hat{\boldsymbol{\theta}} - \boldsymbol{\theta}) \tag{7}$$

where c is a scalar that does not depend on $\hat{\boldsymbol{\theta}}$. From (7), the ML estimates of the vectors $\boldsymbol{r}_S$ and $\boldsymbol{\gamma}_S$ are as follows:

$$\hat{\boldsymbol{r}}_S = [\hat{x}_S, \hat{y}_S, \hat{z}_S]^T = \arg\max_{x,y,z} \ln W(\hat{\boldsymbol{\theta}}|\boldsymbol{r}_S) \tag{8}$$

$$\hat{\boldsymbol{\gamma}}_S = \left[\hat{\alpha}_S, \hat{\beta}_S, \hat{r}_S\right]^T = \arg\max_{\alpha,\beta,r} \ln W(\hat{\boldsymbol{\theta}}|\boldsymbol{\gamma}_S). \tag{9}$$

In practice, the estimates $\hat{\boldsymbol{r}}_S$ and $\hat{\boldsymbol{\gamma}}_S$ can be calculated by using a grid search algorithm that maximizes (8) and (9) in 3-D space over the parameters x, y, and z or α, β, and r, respectively. The areas of admissible values of coordinates $\{x, y, z\}$ or $\{\alpha, \beta, r\}$ should be chosen based on the network geometry and any prior information that is available about the source position. The estimators (8) and (9) are referred to as 3-D MLE.

An important practical problem occurs when a network of compact arrays is applied to localize sources with known depths. Corresponding applications involve localizing surface vessels [1], [2], [9] and monitoring the soundscapes of coral reefs [16] and other shallow water areas. If it is known that surface vessels or marine animals in shallow water habitats are located at constant depths, this information can be used to estimate the positions of these sources. If the variations in depths are much smaller than the range of coordinates x and y, we can assume that the depths of all sources z_S are known. Then, the positions of sources can be estimated in the horizontal plane by using a 2-D grid search algorithm over the parameters x and y only. The corresponding ML estimate is

$$\tilde{\boldsymbol{r}}_S = [\hat{x}_S, \hat{y}_S,\ z_S]^T = \arg\max_{x,y} \ln W(\hat{\boldsymbol{\theta}}|\boldsymbol{r}_S). \tag{10}$$

The estimator (10) is referred to as 2-D MLE. In general, localization of sources with any known coordinate should be performed in the same way by using a grid search over the unknown coordinates.

For the Gaussian measurement errors $\boldsymbol{\varepsilon} = [\varepsilon_{\alpha 1}, \ldots, \varepsilon_{\alpha N}, \varepsilon_{\beta 1}, \ldots, \varepsilon_{\beta N}]^T$, the variances of the ML position estimates (8)–(10) can be approximated by the CRBs. The structures of the CRBs are similar for the rectangular (1) and spherical (2) coordinates of the source. For the spherical coordinates (2), the CRB is derived to be [15], [17]

$$\mathrm{CRB}\,(\boldsymbol{\gamma}) = \boldsymbol{F}(\boldsymbol{\gamma})^{-1} \tag{11}$$

where

$$\begin{aligned}\boldsymbol{F}(\boldsymbol{\gamma}) &= E\left[\left(\frac{\partial \ln W(\hat{\boldsymbol{\theta}}|\boldsymbol{\gamma})}{\partial \boldsymbol{\gamma}}\right)^T \left(\frac{\partial \ln W(\hat{\boldsymbol{\theta}}|\boldsymbol{\gamma})}{\partial \boldsymbol{\gamma}}\right)\right] \\ &= -E\left[\frac{\partial^2 \ln W(\hat{\boldsymbol{\theta}}|\boldsymbol{\gamma})}{\partial \boldsymbol{\gamma} \partial \boldsymbol{\gamma}^{\boldsymbol{T}}}\right] \in R^{3\times 3}\end{aligned} \tag{12}$$

is the Fisher information matrix (FIM). Performing statistical averaging of the likelihood function (7), the elements of the FIM can be represented as follows:

$$(\boldsymbol{F})_{m.n} = \nabla_m^T \boldsymbol{C}^{-1} \nabla_n, \quad m,n = 1,\ldots,3 \tag{13}$$

where

$$\nabla_m = \frac{\partial \boldsymbol{\theta}}{\partial \gamma_m} = \left[\frac{\partial \boldsymbol{\alpha}^T}{\partial \gamma_m}, \frac{\partial \boldsymbol{\beta}^T}{\partial \gamma_m}\right]^T \in R^{2N} \tag{14}$$

is the vector of partial derivatives of the bearings (4) over the parameter γ_m; γ_m is the mth element of the vector $\boldsymbol{\gamma}$ (2); and $(\boldsymbol{F})_{m.n}$ is the (m,n)th element of the FIM (12). Partial derivatives of the azimuths and elevations (14) are given as follows:

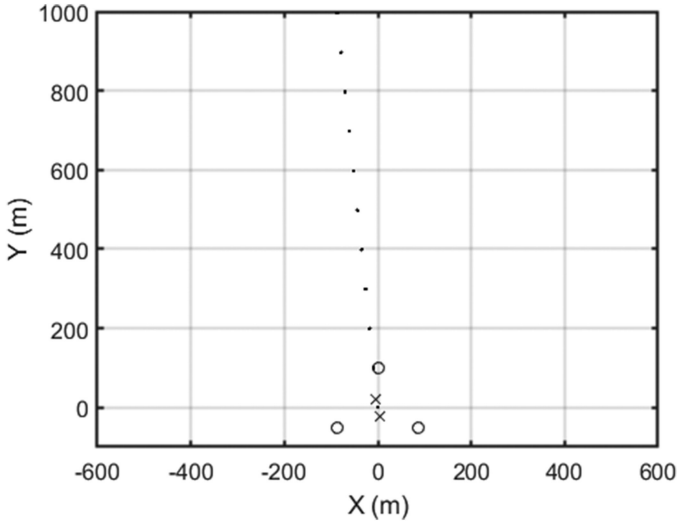

Fig. 1. Locations of compact arrays from the Ocean Network Canada (ONC) with $N = 2$ arrays (symbol "X") and hypothetical network with $N = 3$ arrays (symbol "○") used for simulations. The simulation point positions are shown by dots.

$$\frac{\partial \alpha_n}{\partial \alpha} = \frac{1}{d_n^2}\left[\frac{\partial x}{\partial \alpha}(y - y_n) - \frac{\partial y}{\partial \alpha}(x - x_n)\right] \tag{15a}$$

$$\frac{\partial \beta_n}{\partial \alpha} = \frac{-1}{D_n^2}\frac{\partial d_n}{\partial \alpha}(z - z_n) \tag{15b}$$

$$\frac{\partial \alpha_n}{\partial \beta} = \frac{1}{d_n^2}\left[\frac{\partial x}{\partial \beta}(y - y_n) - \frac{\partial y}{\partial \beta}(x - x_n)\right] \tag{15c}$$

$$\frac{\partial \beta_n}{\partial \beta} = \frac{1}{D_n^2}\left[\frac{\partial z}{\partial \beta} d_n - \frac{\partial d_n}{\partial \beta}(z - z_n)\right] \tag{15d}$$

$$\frac{\partial \alpha_n}{\partial r} = \frac{1}{d_n^2}\left[\frac{\partial x}{\partial r}(y - y_n) - \frac{\partial y}{\partial r}(x - x_n)\right] \tag{15e}$$

$$\frac{\partial \beta_n}{\partial r} = \frac{1}{D_n^2}\left[\frac{\partial z}{\partial r} d_n - \frac{\partial d_n}{\partial r}(z - z_n)\right] \tag{15f}$$

where $D_n^2 = \|\boldsymbol{r}_S - \boldsymbol{r}_n\|^2$ and $d_n^2 = (x - x_n)^2 + (\mathrm{y} - y_n)^2$. Partial derivatives of the coordinates $\{x, y, z\}$ over the parameters $\{\alpha, \beta, r\}$ are as follows:

$$\frac{\partial x}{\partial \alpha} = r\cos\alpha\cos\beta, \quad \frac{\partial y}{\partial \alpha} = -r\sin\alpha\cos\beta, \frac{\partial z}{\partial \alpha} = 0 \tag{16a}$$

$$\frac{\partial x}{\partial \beta} = -r\sin\alpha\sin\beta, \quad \frac{\partial y}{\partial \beta} = -r\cos\alpha\sin\beta, \frac{\partial z}{\partial \beta} = r\cos\beta \tag{16b}$$

$$\frac{\partial x}{\partial r} = \sin\alpha\cos\beta, \quad \frac{\partial y}{\partial r} = \cos\alpha\cos\beta, \frac{\partial z}{\partial r} = \sin\beta. \tag{16c}$$

We obtain representations for the FIM $\boldsymbol{F}(\boldsymbol{\gamma})$ by substituting (16) into (15), (14), and (13). The closed-form representations of the FIM $\boldsymbol{F}(\boldsymbol{r})$ in rectangular coordinates can be obtained similarly by computing partial derivatives (15) over the parameters $\{x, y, z\}$ and substituting them into (14) and (13).

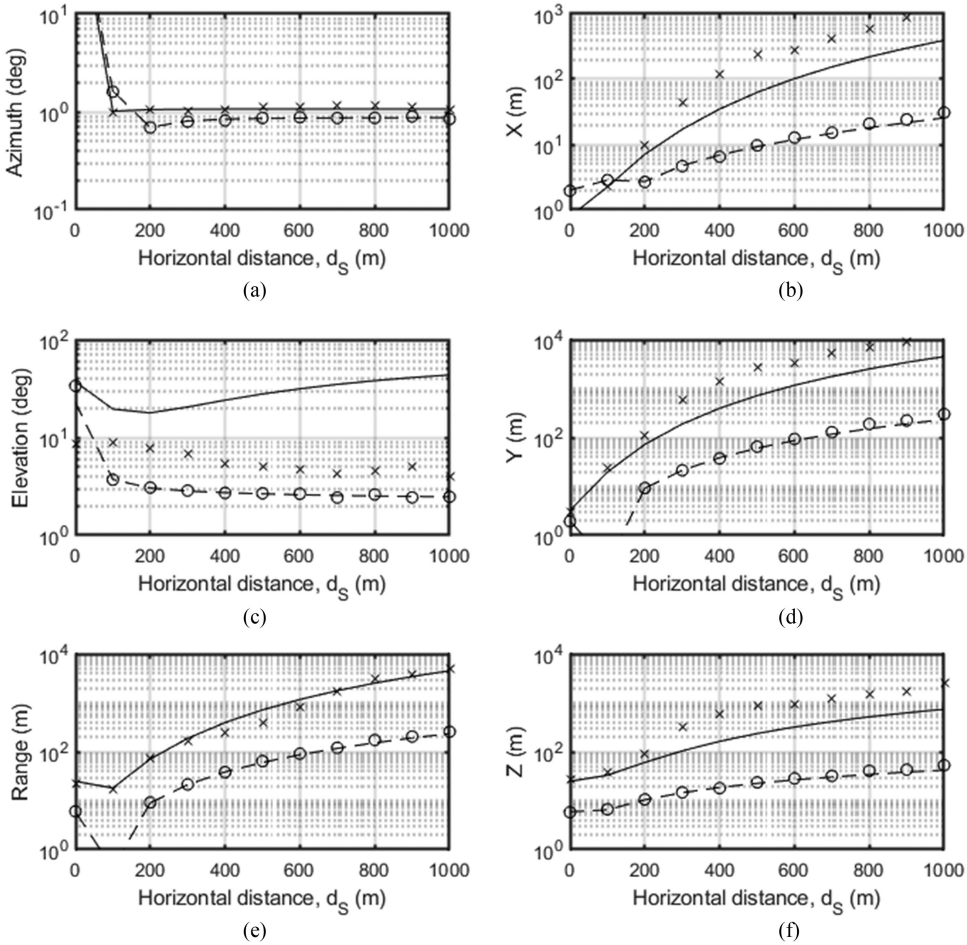

Fig. 2. RMSE of position estimates in polar [(a), (c), and (e)] and rectangular [(b), (d), and (f)] coordinates as functions of a horizontal distance. Empirical RMSEs obtained for the ONC network with $N = 2$ arrays ($D_1 = 43$ m) and the hypothetical network with $N = 3$ arrays ($D_2 = 173$ m) are displayed by symbols "X" and "∘." CRBs (17) are shown by solid ($N = 2$) and dashed ($N = 3$) lines.

The approximations of variances of the estimates $\{\hat{\alpha}_S, \hat{\beta}_S, \hat{r}_S\}$ and $\{\hat{x}_S, \hat{y}_S, \hat{z}_S\}$ can be represented as follows:

$$\sigma_\alpha^2 = E\left\{(\hat{\alpha}_S - \alpha_S)^2\right\} \geq \left(\mathrm{CRB}\left(\boldsymbol{\gamma}\right)\right)_{1,1} \tag{17a}$$

$$\sigma_\beta^2 = E\left\{\left(\hat{\beta}_S - \beta_S\right)^2\right\} \geq \left(\mathrm{CRB}\left(\boldsymbol{\gamma}\right)\right)_{2,2} \tag{17b}$$

$$\sigma_r^2 = E\left\{(\hat{r}_S - r_S)^2\right\} \geq \left(\mathrm{CRB}\left(\boldsymbol{\gamma}\right)\right)_{3,3} \tag{17c}$$

$$\sigma_x^2 = E\left\{(\hat{x}_S - x_S)^2\right\} \geq \left(\mathrm{CRB}\left(\boldsymbol{r}\right)\right)_{1,1} \tag{17d}$$

$$\sigma_y^2 = E\left\{(\hat{y}_S - y_S)^2\right\} \geq \left(\mathrm{CRB}\left(\boldsymbol{r}\right)\right)_{2,2} \tag{17e}$$

$$\sigma_z^2 = E\left\{(\hat{z}_S - z_S)^2\right\} \geq \left(\mathrm{CRB}\left(\boldsymbol{r}\right)\right)_{3,3}. \tag{17f}$$

For surface vessels and other sources with known depths, it makes sense to evaluate the position estimation accuracy in the horizontal plane. The variance of the horizontal position estimate $\{\hat{x}_S, \hat{y}_S\}$ is

$$\sigma_{xy}^2 = \sigma_x^2 + \sigma_y^2. \tag{18}$$

IV. Test Results

In this study, a network of two tetrahedral arrays of underwater recorders was used for statistical simulations and *in situ* tests. Each array consisted of four hydrophones spaced at 1.85 m and sampled by an autonomous multichannel acoustic recorder (AMAR, JASCO Applied Sciences) [9]. Both arrays were deployed on the VENUS cabled ocean observatory operated by Ocean Network Canada, Victoria, BC, Canada, in the Strait of Georgia near Vancouver, BC, Canada. The AMAR had four GeoSpectrum M-36 hydrophones sampled at 64 kHz using the AMAR's four-channel analog-to-digital converter to ensure simultaneous sampling. Combined hydrophone sensitivity and current-to-voltage converter board sensitivity were -165 dB re 1 V/μPa at 250 Hz. The arrays were deployed at the ocean bottom at 168-m depth, and the positions of the array centers were $\boldsymbol{r}_1 = [4.5, -21.2, -168.0]^T$ and $\boldsymbol{r}_2 = [-4.5,\ 21.2,\ -168.0]^T$ m. The aperture of this network was $D_1 = \|\boldsymbol{r}_2 - \boldsymbol{r}_1\| = 43$ m. The array positions and orientations were measured during the deployment and calibrated using surface vessels with known GPS coordinates [8], [9]. Possible errors in orientation and location of the arrays were not

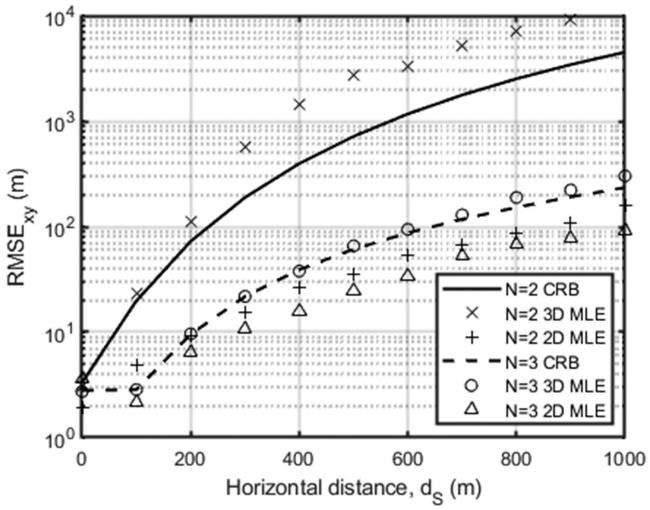

Fig. 3. RMSE of position estimates in a horizontal plane (20) as functions of horizontal distance obtained for a network with $N = 2$ arrays ($D_1 = 43$ m) and $N = 3$ arrays ($D_2 = 173$ m).

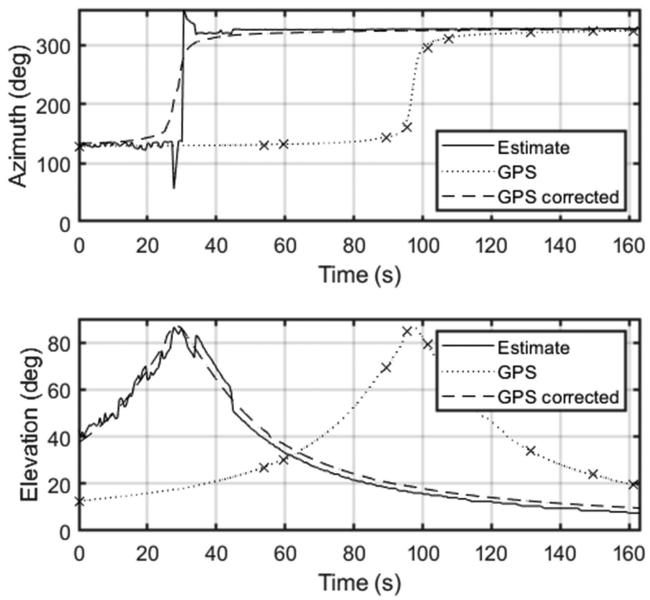

Fig. 4. Bearing estimates, GPS-based bearings, and corrected GPS-based bearings. GPS-based bearings at the AIS time are shown by symbols "X."

accounted for because they are negligibly small as compared to the typical source-to-network distances.

To evaluate the influence of the number of arrays and the distance between them on the localization accuracy, in statistical simulations, we also considered a hypothetical network consisting of three arrays located on a circle with 100-m radius. The coordinates of the arrays were $\boldsymbol{r}_1 = [0, 100, -168.0]^T$, $\boldsymbol{r}_2 = [86.6, -50, -168.0]^T$, and $\boldsymbol{r}_3 = [-86.6, -50, -168]^T$ m. The network aperture was $D_2 = \max_{i,j=1,\ldots,3} \|\boldsymbol{r}_i - \boldsymbol{r}_j\| = 173$ m. The array positions of two networks considered in this paper are shown in Fig. 1.

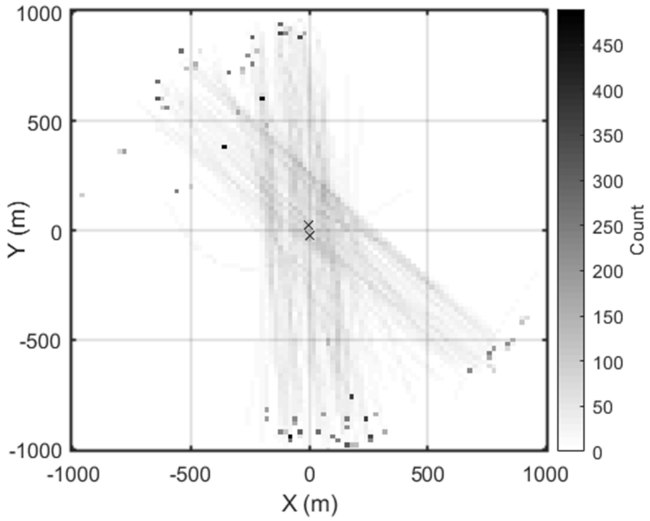

Fig. 5. Spatial distribution of the GPS-based coordinates of 204 vessels. The gray level represents the number of GPS-based coordinates at 20 m × 20 m rectangular bins.

A. Simulations

The goal of the statistical simulations was to compare the accuracy of the ML estimators (7) and (8) with the CRB (17) and evaluate the influence of the array geometry and the horizontal distance of the source on the localization accuracy using the data model presented in Section II. Other sources of errors were outside the scope of this paper and can be a topic of future research. Statistical simulations were conducted for 11 source positions simulating the locations of a source with a known depth. Simulation points had horizontal ranges $d_S = [0, 100, 200, \ldots, 1000]$ m from the origin the depth $z_S = -5$ m, and the azimuth $\alpha_S = -5^\circ$. The horizontal range to the source is given as follows:

$$d_S = \sqrt{x_S^2 + y_S^2}. \tag{19}$$

The positions of simulation points are shown in Fig. 1. For each simulation point, the root-mean-square errors (RMSE) of rectangular (1) and polar (2) coordinates were computed using $L = 1000$ runs. In each run, bearing errors were simulated as a random i.i.d. Gaussian process with zero mean and $\sigma_\alpha = 1.5^\circ$ and $\sigma_\beta = 1.6^\circ$. The values σ_α and σ_β corresponded to the average standard deviation of bearing estimates of vessels obtained in [8] and [9].

The position estimation accuracy of sources with known depth can be evaluated in a horizontal plane. For these sources, the RMSE is given as follows:

$$\mathrm{RMSE}_{xy} = \sqrt{(L)^{-1} \sum\nolimits_{l=1}^{L} \Delta_l^2} \tag{20}$$

where $\Delta_l^2 = (\hat{x}_l - x_S)^2 + (\hat{y}_l - y_S)^2$; $\hat{x}_l$ and $\hat{y}_l$ are the ML estimates (8) or (10) obtained in the lth simulation run.

The first simulation scenario evaluated the dependence of RMSE of the 3-D ML estimates (8) and (9) on the horizontal distance d_S (19). The simulation results are shown in Fig. 2.

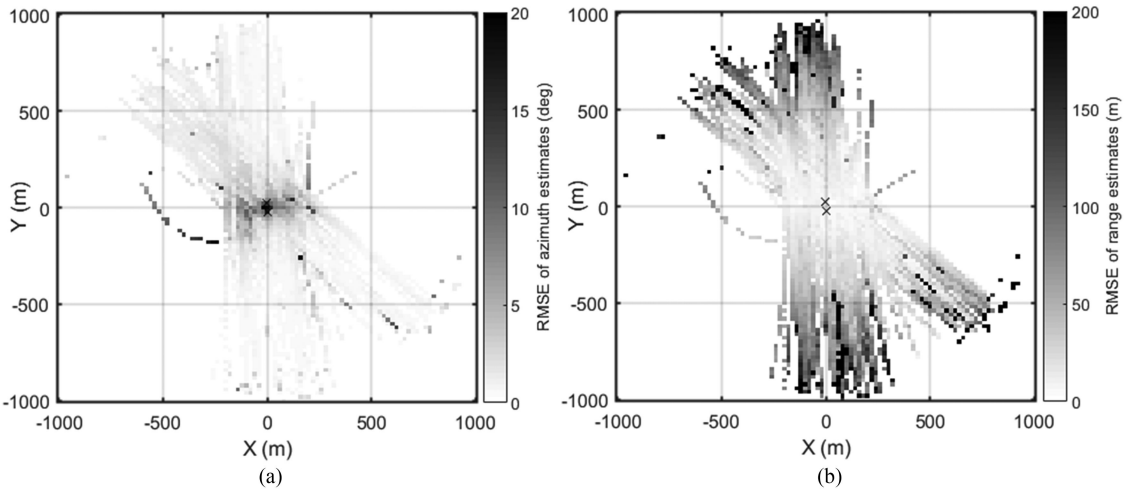

Fig. 6. RMSE of (a) azimuth and (b) range estimates of 204 vessels as a function of vessel positions.

In the second simulation scenario, RMSEs of position estimates in the horizontal plane (20) as functions of horizontal distance d_S (19) were computed for two networks with $N = 2$ arrays and $N = 3$ arrays. The simulation results are shown in Fig. 3.

The third simulation scenario evaluated the influence of prior information about the depth of the source on the RMSE of range and heading estimates. The plots obtained for the 2-D MLE (10) considering the known depth z_S are also shown in Fig. 3 by symbols "+" ($N = 2$) and "Δ" ($N = 3$).

B. In Situ Tests

In situ tests were conducted using a network of two stationary AMARs deployed at the VENUS ocean observatory [9]. We tested the 2-D MLE (10) considering the known depth. Position estimation accuracy was evaluated using 204 vessels traveling near the arrays from February 18 to September 30, 2016. The tests obtained geographic locations and speeds during the passes of these vessels from their AIS broadcasts. The average speed of tested vessels was from 1 to 11 m/s. In each of the *n*th compact arrays, vessel azimuths and elevations were measured using the ML TDOA-based algorithm [9] computing the azimuth and elevation estimates as follows:

$$\left\{\hat{\alpha}\left(t_{nk}\right), \hat{\beta}\left(t_{nk}\right)\right\} = \arg\min_{\alpha,\beta} \sum_i \sum_j \left(\hat{\tau}_{i,j}\left(t_{nk}\right) - \tau_{i,j}\left(\alpha, \beta, d_0\right)\right)^2 \quad n = 1, 2, k = 1, \ldots, K \tag{21}$$

where $\hat{\tau}_{i,j}(t_{nk})$ is the TDOA estimate between the ith and jth recorders of the array ($i = 1, \ldots, 3, j = 2, \ldots, 4$) computed for the time t_{nk}, $\tau_{i,j}(\alpha, \beta, d_0)$ is the expected TDOA computed for the azimuths $\alpha = 0°, \ldots, 360°$, elevation angle $\beta = 0°, ..., 90°$, and range d_0 (the resolution for α and β was 0.5° and the value $d_0 = 500$ m was used in this paper). Index k specifies time instance of the kth bearing measurement. The compact arrays were asynchronous such that $t_{1k} \neq t_{2k}$. However, the maximum time difference between the bearing measurements (21) at different arrays was less than 1 s, $|t_{1k} - t_{2k}| < 1$ s. The TDOAs of vessel noise were computed for consecutive nonoverlapped data segments 1-s long, each in the 50–25 000 Hz frequency range. Vessel positions were independently estimated in the horizontal plane using the ML estimator (10) and a grid search algorithm in the 2-D space over the parameters $x = [-2000 : 5 : 2000]$ m, $y = [-2000 : 5 : 2000]$ m, and $z = -5$ m.

The true vessel positions were computed by interpolating the AIS-based GPS coordinates $\boldsymbol{r}_{\mathrm{GPS}}(t)$ for the time samples $t_{1k} \approx t_{2k},\ k = 1, \ldots, K$. We assumed that the dominant source of vessel noise arises from propulsion systems, and that the acoustic measurements (3) and (5) correspond to the average bearing of these components. For large commercial vessels, the average position of these components $\boldsymbol{r}_P(t)$ can differ from the positions broadcasted through AIS, which are derived from GPS devices with antennas that can be mounted elsewhere on the vessel, at $\boldsymbol{r}_{\mathrm{GPS}}(t_k)$. However, both the noise source and the GPS antenna travel in the same trajectory, $\boldsymbol{r}_P(t_k) = \boldsymbol{r}_{\mathrm{GPS}}(t_k - \tau_P)$. The time delay τ_P and corresponding source position $\boldsymbol{r}_P(t_k)$ were obtained from the measured bearings and the GPS-based bearings using a least mean square algorithm as

$$\hat{\tau}_p = \arg\min_{\tau} \rho\left(\tau\right) \tag{22}$$

where $\rho(\tau) = \sum_k \left(\hat{\beta}_{1k} - \beta(t_k - \tau)\right)^2$, where $\hat{\beta}_{1k}$ is the elevation estimate (4) of a vessels computed using the first array and $\beta(t_k)$ is the GPS-based elevation at time t_k. Fig. 4 shows an example of bearing estimates, GPS-based bearings, $\boldsymbol{r}_{\mathrm{GPS}}(t_k)$, and corrected GPS-based bearings of a vessel, $\boldsymbol{r}_{\mathrm{GPS}}(t_k - \hat{\tau}_P)$.

Fig. 5 shows the spatial distribution of all available corrected GPS-based vessel coordinates. In this figure, the gray level represents the number of GPS-based coordinates at 20 m × 20 m rectangular bins.

To evaluate the performance of the 2-D MLE (10), the robust version of the RMSE (20) using the median value of square errors

$$\mathrm{RMSE}_{xy} = \sqrt{\mathrm{median}\left\{\Delta_k^2\right\}} \tag{23}$$

was computed independently for each bin with ten or more measurements. Here, $\Delta_k^2 = (\hat{x}_k - x_S)^2 + (\hat{y}_k - y_S)^2$, where $\hat{x}_k$ and $\hat{y}_k$ are the ML estimates (10) obtained at the kth time

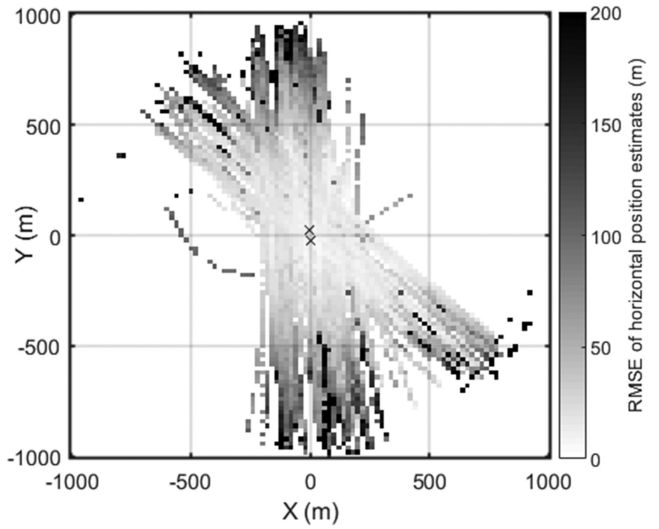

Fig. 7. RMSE of position estimates of 204 vessels in horizontal plane.

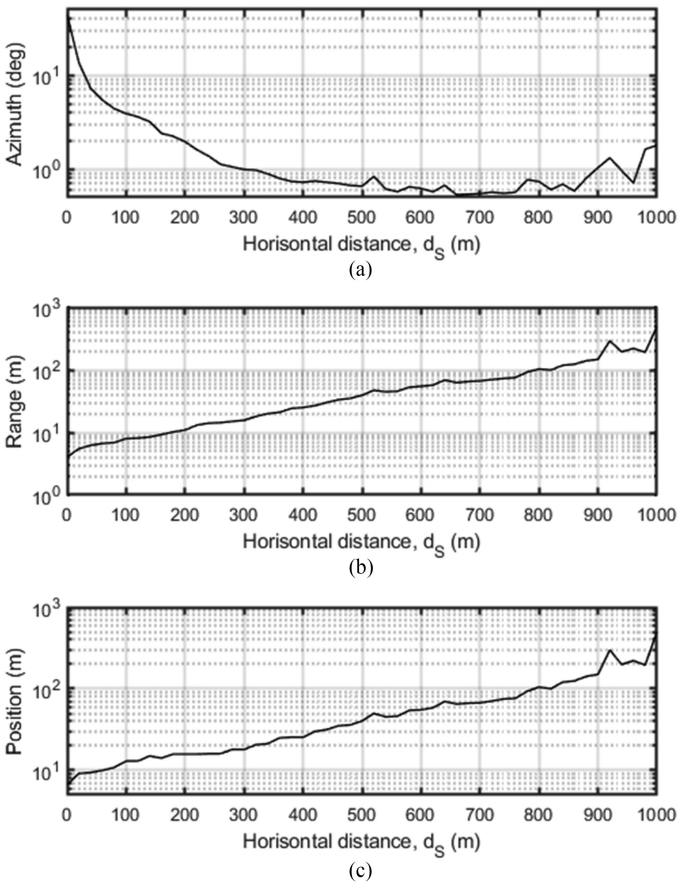

Fig. 8. RMSE of (a) azimuth estimates, (b) range estimates, and (c) position estimates in horizontal plane as a function of a horizontal distance d_S.

instance t_k. If the error has a Gaussian distribution, then the median square error (23) is equal to the mean square error (20), which, in turn, matches with the variance (18) if the position estimates are unbiased. However, the median estimate (23) is unaffected by outliers compared to the mean square errors (20). The robust RMSE (23) of azimuth and range estimates in the 2-D space are shown in gray in Fig. 6, and RMSE of the source position estimates in horizontal plane are shown in gray in Fig. 7.

We also evaluated the RMSE of azimuth, range, and position estimates in the horizontal plane as a function of a horizontal distance d_S (19). The results are shown in Fig. 8.

V. Discussions and Conclusion

The results of statistical simulations demonstrate that in the case of Gaussian bearing errors, the RMSE of the position estimates (8) and (9) obtained by searching in the 3-D space can be approximated by the CRBs. Figs 2 and 3 show that the approximation accuracy is higher for the network consisting of $N = 3$ compact arrays than for the network consisting of $N = 2$ compact arrays. Increasing the number of compact arrays and the distance between them increases the position estimation accuracy.

An important result of statistical simulations and *in situ* tests is that in the case of known coordinate z_S, the empirical RMSE provided by the 2-D MLE (10) is smaller than the CRB [see Figs. 3, 7, and 8(c)]. A similar result was obtained when estimating elevation angles within the admissible range from 0° to 90° using a network of two arrays [see Fig. 2(c)]. These results can be explained by the fact that the CRB values are unlimited, whereas the known range of possible source coordinates restricts the search area. Having prior information about the source coordinates makes it possible to obtain "superefficient" estimates with RMSE lower than the CRB. This is important for shallow water applications when changes in depth of all sources are not significant, as well as for localization of vessels and other sources with known depth. The accuracy of localizing sources with unknown depth in deep water, such as diving marine mammals, when all three coordinates may vary in a wide range, should be close to the corresponding CRB (see Fig. 2).

The real localization accuracy obtained in *in situ* tests was similar to the simulation results. The increase in the RMSE of azimuth estimates in areas perpendicular to the line connecting the arrays was observed [see Fig. 6(a)]. This is explained by the fact that moving sources were used to evaluate the localization accuracy. The source traveling with the speed v at the distance r_i from the *i*th recorder of the *n*th compact array has an angular velocity of

$$\omega_i = \frac{v \sin \vartheta_n}{r_i} \tag{24}$$

where ϑ_n is the angle between the vectors of source speed and its cross-radial component. Since moving sources have different radial velocities at different recorders of a compact array, they produce different Doppler shifts of sounds received by the recorders. As follows from (24), the highest angular velocity and azimuth rate of the source is reached near its closest point of approach (CPA) when ϑ_n is close to 90°. It resulted in an increase in TDOA-based azimuth estimation errors near the CPA [see Fig. 4(a), time interval between 25 and 32 s]. Thus, high azimuth estimation errors may occur in the areas with high angular speed of the sources [see Fig. 6(a)]. However, this fact did

not affect the accuracy of vessel position estimates in horizontal plane [see Fig. 7 and 8(c)].

The results of this study demonstrate that using a network of multiple stationary compact arrays can be extremely beneficial to many applications associated with long-term passive acoustic monitoring of vessels and marine mammals over large areas. In addition to the standard tasks of detecting signals and classifying sources, networks of compact arrays make it possible to accurately count the number of sources [18] and estimate their positions. The accuracy of position estimates strongly depends on the number of compact arrays, the distance between them, and prior information about the source coordinates available.

The results from this paper make it possible to implement the ML localization algorithms in multiple compact arrays and to evaluate their performance before the arrays are deployed. However, this paper has omitted many important issues, such as using different array processing techniques [15] to estimate bearings of sources, the influence of bearing estimation accuracy on the accuracy of localization, and the possibility to use multiple compact arrays to track sources. These issues should be researched in the future work.

ACKNOWLEDGMENT

The authors would like to thank the Port of Vancouver for its support of the data acquisition project through the Enhancing Cetacean Habitat and Observation program, Ocean Networks Canada for maintaining the VENUS undersea data network, and the JASCO field team for deploying the compact arrays. The authors also would like to thank K. Hiltz for editing a draft version of the manuscript and two anonymous reviewers for their comments that helped to improve the quality of this paper.

REFERENCES

[1] K. W. Chung, A. Sutin, A. Sedunov, and M. Bruno, "DEMON acoustic ship signature measurements in an urban harbor," *Adv. Acoust. Vib.*, vol. 2011, 2011, Art. no. 952798.

[2] A. Tesei, S. Fioravanti, V. Grandi, P. Guerrini, and A. Maguer, "Localization of small surface vessels through acoustic data fusion of two tetrahedral arrays of hydrophones," *Proc. Meetings Acoust.*, vol. 17, 2012, Art. no. 070050.

[3] S. M. Wiggins, M. A. McDonald, and J. A. Hildebrand, "Beaked whale and dolphin tracking using a multichannel autonomous acoustic recorder," *J. Acoust. Soc. Amer.*, vol. 131, pp. 156–163, 2012.

[4] M. Y. R. Hirotsu, T. Ura, M. Sakata, H. Sugimatsu, J. Kojima, and R. Bahl, "Localization of sperm whales in a group using clicks received at two separated short baseline arrays," *J. Acoust. Soc. Amer.*, vol. 127, pp. 133–147, Jan. 2010.

[5] S. M. Wiggins, K. E. Frasier, E. E. Henderson, and J. A. Hildebrand, "Tracking dolphin whistles using an autonomous acoustic recorder array," *J. Acoust. Soc. Amer.*, vol. 133, pp. 3813–3818, 2013.

[6] M. Gassmann, E. E. Henderson, S. M. Wiggins, M. A. Roch, and J. A. Hildebrand, "Offshore killer whale tracking using multiple hydrophone arrays," *J. Acoust. Soc. Amer.*, vol. 134, pp. 3513–3521, 2013.

[7] M. Gassmann, S. M. Wiggins, and J. A. Hildebrand, "Three-dimensional tracking of Cuvier's beaked whales' echolocation sounds using nested hydrophone arrays," *J. Acoust. Soc. Amer.*, vol. 138, pp. 2483–2494, 2015.

[8] I. R. Urazghildiiev and D. Hannay, "Maximum likelihood estimators and Cramér–Rao bound for estimating azimuth and elevation angles using compact arrays," *J. Acoust. Soc. Amer.*, vol. 141, pp. 2548–2555, 2017.

[9] I. R. Urazghildiiev and D. E. Hannay, "Using a stationary compact array of acoustic sensors to estimate the motion parameters of sources," *IEEE J. Ocean. Eng.*, vol. 43, no. 4, pp. 1134–1142, Oct. 2018.

[10] Y. Bar-Shalom and X.-R. Li, *Estimation and Tracking: Principles, Techniques, and Software*. Norwood, MA, USA: Artech House, 1993.

[11] D. Mušicki, "Bearings only multi-sensor maneuvering target tracking," *Syst. Control Lett.*, vol. 57, pp. 216–221, 2008.

[12] S. M. Wiggins, M. A. McDonald, and J. A. Hildebrand, "Beaked whale and dolphin tracking using a multichannel autonomous acoustic recorder," *J. Acoust. Soc. Amer.*, vol. 131, pp. 156–163, 2012.

[13] S. M. Wiggins, K. E. Frasier, E. E. Henderson, and J. A. Hildebrand, "Tracking dolphin whistles using an autonomous acoustic recorder array," *J. Acoust. Soc. Amer.*, vol. 133, pp. 3813–3818, 2013.

[14] M. Gassmann, S. M. Wiggins, and J. A. Hildebrand, "Three-dimensional tracking of Cuvier's beaked whales' echolocation sounds using nested hydrophone arrays," *J. Acoust. Soc. Amer.*, vol. 138, pp. 2483–2494, 2015.

[15] H. L. Van Trees, *Optimum Array Processing: Part IV of Detection, Estimation, and Modulation Theory*. Hoboken, NJ, USA: Wiley, 2004.

[16] L. A. Freeman and S. E. Freeman, "Rapidly obtained ecosystem indicators from coral reef soundscapes," *Mar. Ecol. Prog. Ser.*, vol. 561, pp. 69–82, 2016.

[17] S. M. Kay, *Fundamentals of Statistical Signal Processing, Volume I: Estimation Theory*. Noida, India: Pearson Educ. India, 1993.

[18] I. R. Urazghildiiev and D. E. Hannay, "Passive acoustic detection and estimation of the number of sources using compact arrays," *J. Acoust. Soc. Amer.*, vol. 143, pp. 2825–2833, 2018.

Ildar R. Urazghildiiev received the M.Sc. degree in electrical engineering from the Zhitomir Institute of Radioelectronics, Zhitomir, Ukraine, in 1989, and the Ph.D. degree in electrical engineering from the National R&D Center of Defense Technologies and Military Security of Ukraine, Kiev, Ukraine, in 1996.

From 1994 to 2001, he was with the National R&D Center of Defense Technologies and Military Security of Ukraine and the National Technical University of Ukraine "Kiev Polytechnic Institute," Kiev, Ukraine. In 2001 and 2003, he held Postdoctoral Fellow positions in the Signals and Systems Group, Uppsala University, Uppsala, Sweden. From 2004 to 2014, he was a Research Associate with the Lab of Ornithology, Cornell University, Ithaca, NY, USA. In 2014, he joined JASCO Applied Sciences, Inc., where he is currently a Senior Research Engineer. His research interests include statistical signal processing, signal detection, parameter estimation, classification, localization, and tracking with applications to bioacoustics.

David E. Hannay received the B.Sc. and M.Sc. degrees in physics from the University of Victoria, Victoria, BC, Canada, in 1988 and 1994, respectively.

He has been a Research Scientist with JASCO Applied Sciences, Victoria, BC, Canada, since 1989, specializing in underwater acoustic modeling for environmental noise assessments. He is currently the Chief Science Officer for JASCO's multinational science teams. He develops computer models for predicting acoustic pressure and particle velocity, and applies those to a variety of industrial noise sources including sonars, explosives, aircraft, seismic exploration sources, shipping, and pile driving. His recent work is related to ship noise measurements and quieting technologies.